



# Kent Academic Repository

Wang, Tianyu, Yan, Yong, Wang, Lijuan, Hu, Yonghui and Zhang, Shuai  
(2020) *Instantaneous Rotational Speed Measurement Using Image Correlation  
and Periodicity Determination Algorithms*. IEEE Transactions on Instrumentation  
and Measurement, 69 (6). pp. 2924-2937. ISSN 0018-9456.

## Downloaded from

<https://kar.kent.ac.uk/75812/> The University of Kent's Academic Repository KAR

## The version of record is available from

<https://doi.org/10.1109/TIM.2019.2932154>

## This document version

Author's Accepted Manuscript

## DOI for this version

## Licence for this version

UNSPECIFIED

## Additional information

## Versions of research works

### Versions of Record

If this version is the version of record, it is the same as the published version available on the publisher's web site.  
Cite as the published version.

### Author Accepted Manuscripts

If this document is identified as the Author Accepted Manuscript it is the version after peer review but before type setting, copy editing or publisher branding. Cite as Surname, Initial. (Year) 'Title of article'. To be published in *Title of Journal*, Volume and issue numbers [peer-reviewed accepted version]. Available at: DOI or URL (Accessed: date).

## Enquiries

If you have questions about this document contact [ResearchSupport@kent.ac.uk](mailto:ResearchSupport@kent.ac.uk). Please include the URL of the record in KAR. If you believe that your, or a third party's rights have been compromised through this document please see our [Take Down policy](https://www.kent.ac.uk/guides/kar-the-kent-academic-repository#policies) (available from <https://www.kent.ac.uk/guides/kar-the-kent-academic-repository#policies>).

Title: Instantaneous Rotational Speed Measurement Using Image Correlation and  
Periodicity Determination Algorithms

Authors: Tianyu Wang <sup>a, b</sup>  
Yong Yan <sup>c</sup> (Corresponding author)  
Lijuan Wang <sup>c</sup>  
Yonghui Hu <sup>a, b</sup>  
Shuai Zhang <sup>a, b</sup>

Addresses: <sup>a</sup> State Key Laboratory of Alternate Electrical Power Systems with Renewable  
Energy Sources, North China Electric Power University, Beijing 102206, China

<sup>b</sup> School of Control and Computer Engineering, North China Electric Power  
University, Beijing 102206, China

<sup>c</sup> School of Engineering and Digital Arts, University of Kent, Canterbury, Kent CT2  
7NT, U.K.

Tel: 00441227823015

Fax: 00441227456084

Email: [y.yan@kent.ac.uk](mailto:y.yan@kent.ac.uk)

## **ABSTRACT**

Dynamic and accurate measurement of instantaneous rotational speed is desirable in many industrial processes for both condition monitoring and safety control purposes. This paper presents a novel imaging based system for instantaneous rotational speed measurement. The low-cost imaging device focuses on the side surface of a rotating shaft without the use of a marker, entailing benefits of non-contact measurement, low maintenance and wide applicability. Meanwhile, new periodicity determination methods based on the Chirp-Z transform and parabolic interpolation based auto-correlation algorithm are proposed to process the signal of similarity level reconstructed using an image correlation algorithm. Experimental investigations are conducted on a purpose-built test rig to quantify the effects of the periodicity determination algorithm, frame rate, image resolution, exposure time, illumination conditions, and photographic angle on the accuracy and reliability of the measurement system. Experimental results under steady and transient operating conditions demonstrate that the system is capable of providing measurements of a constant or gradually varying speed with a relative error no greater than  $\pm 0.6\%$  over a speed range from 100 to 3000 RPM (Revolutions Per Minute). Under step change conditions the proposed system can achieve valid speed measurement with a maximum error of 1.4%.

**Index Terms**– Instantaneous rotational speed; Tachometer; Image processing; Image correlation; Spectral analysis; Autocorrelation.

## **I. INTRODUCTION**

Rotating machineries are widely seen in a range of industrial sectors such as energy, power, transportation and manufacturing industries. The instantaneous rotational speed of a rotating

machine usually carries a great deal of useful information about its operating conditions [1-3]. For instance, the fault of a rolling-element bearing due to the local abrasion of outer and inner raceways can be identified by analyzing the variations in the rotational speed [3, 4]. The impulse components due to the inner collision or vibration are usually embedded in the speed signal [4]. In a modern vibration based system for condition monitoring and fault diagnosis, instantaneous rotational speed is one of the most important parameters to be measured [5]. Therefore, accurate and dynamic measurement of instantaneous rotational speed is a pre-requisite in the smart condition monitoring and diagnosis of rotating machineries. There are a range of techniques available for rotational speed measurement [6-12]. However, each technique has its advantages and fundamental limitations and cannot perform well under all industrial conditions. Mechanical tachometers, such as centrifugal tachometers or multi-gear disk-based tachometers, commonly suffer from mechanical wear during long-time operation. Photoelectric tachometers are able to achieve high measurement accuracy and high resolution, but the presence of dust around the delicate optical components restricts their wide applicability in a hostile environment [7]. Electrostatic sensors cannot perform well at low speeds due to insufficient electrostatic charge generated on the rotor surface [8]. The magnetic tachometers are unsuitable for nonmagnetic materials due to the nature of magnetic sensing principle [9]. In addition, many attempts have been made to derive the instantaneous rotational speed of the induction motor from a motor current signal without the use of a tachometer [10, 11]. Over the last few years, the accelerometers in conjunction with vibration signal processing algorithms have been proposed to estimate the instantaneous angular speed [5, 12]. However, such systems are unsuitable for accurate rotational speed measurement in some industrial applications. The significant noise involved in the vibration signal will generate severe spectral interference and hence affect the measurement accuracy [12].

Although various tachometers are commercially available, their applicability is limited due to the costly installation and maintenance of sensors along with dedicated wirings, especially for the hazardous mechanical systems. In consideration of relatively short measurement distances of existing tachometers, they may not be suitable for some industrial applications. In addition, most conventional tachometers are point-wise sensors originally designed for collecting single speed data streams. To address these problems, substantial endeavors have been made to develop new techniques that can advance the current state-of-the-art in instantaneous rotational speed measurement.

With rapid advances in imaging sensors and image processing algorithms in recent years, imaging based techniques provide a promising alternative to rotational speed measurement [13-21]. The imaging technique is potentially suitable for applications in a hostile environment because of its sensing principle. The imaging device can be set up at a remote location even hundreds of meters away. Since the imaging sensor has no direct contact with the rotor, there is no wear problem that adversely affects some of the existing techniques such as mechanical tachometers. In addition, the imaging sensor can be regarded as a full-field measuring technique simultaneously tracking multiple points on a rotating object and thus providing multi-channel data as well as other essential variables such as vibration mode [22], realizing systematic condition monitoring and process control. Imaging systems for rotational speed measurement are expected to find applications in many industrial fields, for instance, the condition monitoring of large-scale rotating machines under high-temperature or high-radiation environments such as gas turbines or wind turbines. For the image series of a moving object, the intensity variation of pixels is the reflection of the motion of the object [23]. Existing speed measurement systems based on the imaging principle are normally implemented by exploiting the intensity distribution difference between two consecutive frames

with the aid of camera calibration techniques [13-18]. An instantaneous rotational speed measurement system using a high-speed camera and a well-designed varying-density fringe pattern was proposed by Zhong *et al.* [13, 14]. The imaged fringe pattern intensity changed due to the rotation of the shaft, from which the instantaneous rotational speed was obtained. Kim *et al.* [15] used a high-speed camera with a switching colour pattern on the rotating shaft for rotational speed measurement. Li *et al.* [17] proposed a vision-based method to measure the rotational angle using a calibration pattern with a spot array. Previously reported imaging approaches are normally implemented through tracking high-contrast markers or speckle patterns on the rotating surface. In this case, high-speed cameras with a minimum frame rate of 800 fps (frames per second) are usually required to acquire clear images to reduce the impacts of motion blur and hence correctly recognize the artificial marker. The measurement accuracy of such methods is closely associated with the image resolution. A better measurement performance requires a higher image resolution. The low affordability of high-speed and high-resolution cameras limits the wide application of such systems. It is therefore desirable to develop techniques that use low-cost imaging devices to achieve accurate rotational speed measurements.

In their previous research the authors of this paper have developed a low-cost imaging technique for rotational speed measurement through image similarity evaluation and spectral analysis [19, 20]. However, a marker is required to be fixed on the surface of a rotor. It is difficult to meet this requirement in some industrial applications. In this paper the imaging system for rotational speed measurement focuses on the side surface of the shaft without any markers. Such a system requires lower maintenance and has wider applicability than the marker based systems. Moreover, new methods for periodicity determination based on the Chirp-Z transform (CZT) and parabolic interpolation based auto-correlation (PIAC) are proposed to determine the rotational speed. These

methods transform the problem of estimating the rotational speed into that of determining the period of the image similarity signal. There are very few reports on this topic in the literature. Preliminary studies were first reported at the 2018 IEEE International Instrumentation and Measurement Technology Conference [21]. However, this original system only aims at mean rotational speed measurement under steady states. This paper gives a detailed description of the measurement principle, key aspects of design and implementation, and performance assessment of the measurement system on a PC. Additionally, dynamic measurement of instantaneous rotational speed under time-varying operating conditions is also included. Comparative assessments between the two signal processing methods for periodicity determination are conducted. Moreover, the effects of relevant factors such as frame rate, image resolution, exposure time, illumination conditions, and photographic angle on the performance of the measurement system are quantified and discussed through a comparison to the references from the contact-type rotary encoder and from the laser tachometer.

## **II. MEASUREMENT PRINCIPLE AND METHODOLOGY**

### *A. Measurement Principle*

In this rotational speed measurement system, an imaging device (Basler acA800-510um at a cost of about USD\$500) is placed perpendicular to the axis of the shaft. The intensity variation of the pixels in the image reflects the motion of the rotor, which is the measurement principle of image intensity based method [23]. In this case, the intensity distribution of the acquired images is dependent on a variety of factors, including surface properties of the shaft (i.e. surface roughness, natural pattern, temperature etc.), illumination conditions and background. However, since the time window of each measurement cycle is 1 second for lower speeds (100-1000 RPM) and 0.5

second for higher rotational speeds (1000-3000 RPM), the changes in the shaft temperature and other operational and environmental factors during the short time cycle are insignificant. For certain operating and environment conditions, the image intensity distribution is mainly determined from the natural texture of the rotor surface. During the rotor operation, different parts of the rotor side face are imaged on the sensor plane at different times. Therefore, the intensity distribution of the rotor images varies with time due to the inherent non-uniformity of the rotor surface. The grayscale distribution contains motion information about the rotating shaft and thus its rotational speed is measured from the periodicity of the image intensity distribution.

### *B. Image correlation*

Image correlation is a method for establishing the degree of probability that a linear relationship exists between two measured image matrixes [24]. It directly provides the similarity level between two images with the same size by comparing the intensity distributions of the images during the rotating shaft operation. For two images  $X$  and  $Y$  with a resolution of  $m \times n$  pixels, the correlation coefficient  $r$  is defined as:

$$r = \frac{\sum_{i=1}^m \sum_{j=1}^n [X(i, j) - \bar{X}][Y(i, j) - \bar{Y}]}{\sqrt{\sum_{i=1}^m \sum_{j=1}^n [X(i, j) - \bar{X}]^2 \sum_{i=1}^m \sum_{j=1}^n [Y(i, j) - \bar{Y}]^2}} \quad (1)$$

where  $X(i, j)$  and  $Y(i, j)$  are the gray-scale values at the point  $(i, j)$  in the images  $X$  and  $Y$ , respectively.

$\bar{X}$  and  $\bar{Y}$  are the mean intensity values of the matrices  $X$  and  $Y$ , respectively. It is worth noting that, if the intensity distributions of the test images undergo a linear transformation, the obtained correlation coefficient remains unchanged. Therefore, the correlation coefficient is insensitive to the uniform variations in illumination conditions [25]. The larger the correlation coefficient, the

higher the similarity level between the two images. With the continuous processing of the images, the similarity level of the sequential images is regarded as a time-domain signal.

### *C. Determination of rotational speed*

Under dynamic operating conditions, the reconstructed signal indicating the similarity level has time-varying characteristics. Inspired by time-frequency analysis methods, especially short-time Fourier transform, a sliding short-time window is used to segment the similarity level signal in this study. The  $i^{\text{th}}$  segment of the signal sub-divided by a short-time window can be defined as:

$$S_i(t) = S(t)\omega(t - iT_d) \quad (2)$$

where  $S(t)$  is the resulting signal indicating the similarity level,  $T_d$  is the time shift between two successive segments.  $\omega(t-iT_d)$  is the short-time window function centered at time  $t=iT_d$ , which moves along time to slice the image similarity signal. In the processing, the time shift  $T_d$  is set to 0.2 second and a Gaussian window with a length of one second is chosen to minimize the effect of leakage and picket fence. Then, instantaneous rotational speed is obtained from the periodicity of the signal segment  $S_i(t)$  through the use of periodicity determination methods. Due to the low frame rate of a low-cost imaging device, common methods for periodicity determination, such as Fast Fourier Transform and auto-correlation, do not perform well with limited sampling time [26, 27]. In order to improve the measurement accuracy and resolution of the low-cost imaging system, CZT and PIAC are deployed and compared in this study.

#### *1) Chirp-Z transform*

The main frequency of the signal segment indicating the similarity level is equal to the rotational frequency, which is determined through CZT in this study. The location of the dominate peak is corresponding to the instantaneous rotational frequency of the  $i^{\text{th}}$  signal segment,  $f_i$ , which is then converted into the instantaneous rotational speed:

$$N_i = 60f_i \quad (3)$$

where the instantaneous rotational frequency,  $f_i$ , is given in the unit of Hz, which is equivalent to the instantaneous rotational speed in RPS (Revolutions Per Second). In this study, we use the common unit of an instantaneous rotational speed, RPM (Revolutions Per Minute), which is equivalent to 60 RPS.

The instantaneous rotational frequency  $f_i$  is given in Hz, which is equivalent to the instantaneous rotational speed in RPS (Revolutions Per Second). In this study we have used the common unit of an instantaneous rotational speed, RPM (Revolutions Per Minute), which is equivalent to 60 RPS. CZT is an effective frequency determination method, which allows spectral analysis to be carried out in a limited frequency band with a considerably higher resolution than is obtainable via Fourier transform [27]. A detailed performance comparison of different frequency estimation methods in [28] shows that the Chirp-Z transform is the most suitable method to explore the peak response of a non-stationary signal with a short-time observation window. In this case, the Chirp-Z transform is performed on each segmented signal of similarity level. Given the  $i^{\text{th}}$  signal segment of similarity level  $S_i(t)$ , its Chirp-Z transform  $R_i(m)$  is defined as

$$R_i(m) = \sum_{k=1}^N S_i(k) Z_M^{mk} \quad (m = 0, 1, \dots, M-1) \quad (4)$$

where  $S_i(k)$  ( $k=1, 2, \dots, N$ ) represents the digitalized version of the  $i^{\text{th}}$  signal segment  $S_i(t)$ .  $M$  is the number of sampling points in the Chirp-Z transform with any possible positive integer value.  $Z_M^{mk}$  is the transformation kernel and is calculated as

$$Z_M^{kn} = \exp \left\{ -j \frac{2\pi n}{f_s} \left[ f_0 + \frac{(f_{i1} - f_{i0})k}{M} \right] \right\} \quad (5)$$

where  $f_s$  is the sampling frequency and  $[f_{i0}, f_{i1}]$  is the frequency observation interval, which is the priori information about the rough range of the instantaneous rotational frequency. In this study,  $f_{i0}$  and  $f_{i1}$  are given, respectively, by

$$f_{i0} = f_{iF} - \frac{f_s}{N}, f_{i1} = f_{iF} + \frac{f_s}{N} \quad (6)$$

where  $f_{iF}$  is the preliminary frequency estimate of the  $i^{\text{th}}$  segment, which is calculated as the frequency with the highest amplitude in the frequency spectrum of the segmented signal through the fast Fourier transform algorithm.

Once the Chirp-Z transform  $R_i(m)$  is obtained, the maximum amplitude of the high-resolution frequency spectrum corresponds to the main frequency component of the  $i^{\text{th}}$  signal segment, which is regarded as the fine instantaneous rotational frequency  $f_i$ . The frequency resolution  $\Delta f_c$  of the Chirp-Z transform is dependent upon the length of the frequency observation band and the number of frequency elements covered in the frequency observation band.  $\Delta f_c$  is defined as

$$\Delta f_c = \frac{f_{i1} - f_{i0}}{M} \quad (7)$$

According to equation (3) and (6), the resolution of the rotational speed is determined by

$$\Delta N = 60\Delta f_c = \frac{120f_s}{MN} \quad (8)$$

## 2) Parabolic interpolation based auto-correlation

The period of the  $i^{\text{th}}$  segmented signal of similarity level  $S_i(k)$  ( $k=1, \dots, N$ ) is equal to the period of the rotational motion. The period can be estimated from the auto-correlation function of the segmented signal. A normalized auto-correlation function is defined as

$$R_i(m) = \frac{\sum_{k=1}^N S_i(k)S_i(k+m)}{\sum_{k=1}^N S_i^2(k)} \quad (9)$$

where  $N$  is the number of points in the correlation computation.  $m$  ( $m=0 \dots, N$ ) is the number of delayed points. The normalized auto-correlation function is used to obtain the correlation coefficient, namely the value of the dominate peak (other than the unity at  $m = 0$ ). The location of the peak on the time axis of the auto-correlation function is the coarse rotation period.

However, the period may not be located at the discrete points in the auto-correlation function. In the measurement system using a low-cost camera, the performance of the auto-correlation algorithm is limited by a relatively low frame rate (below 500fps), which can lead to significant errors in period estimation. Therefore, an effective interpolation strategy, i.e. parabolic interpolation of the peak in the auto-correlation function is employed to generate a closer approximation to the actual rotational period. This interpolation method determines a fine peak by fitting a parabola through three sampling points around the coarse peak [29]. This approach has been commonly used in time delay estimation due to high accuracy and low computational complexity. In this case, the abscissas of three samples  $P_1(x_1, y_1)$ ,  $P_2(x_2, y_2)$  and  $P_3(x_3, y_3)$  used for parabolic interpolation, which are located on the time axis of the auto-correlation function with the corresponding ordinates being the correlation coefficient, are obtained from equations, respectively

$$x_1 = \tau_i - \frac{1}{f_s} \quad (10)$$

$$x_2 = \tau_i \quad (11)$$

$$x_3 = \tau_i + \frac{1}{f_s} \quad (12)$$

where  $\tau_i$  is the coarse estimate of the rotational period of the  $i^{\text{th}}$  segment determined from the auto-correlation function.  $f_s$  is the frame rate of the imaging device. The parabola that fits these points is obtained from

$$y = ax^2 + bx + c \quad (13)$$

with the parabola coefficients as follows

$$a = \frac{(x_1 - x_3)(y_1 - y_2) - (x_1 - x_2)(y_1 - y_3)}{(x_1 - x_2)(x_1 - x_3)(x_2 - x_3)} \quad (14)$$

$$b = \frac{(y_1 - y_2) - a(x_1 - x_2)^2}{(x_1 - x_2)} \quad (15)$$

$$c = y_1 - ax_1^2 - bx_1 \quad (16)$$

Consequently, the fine rotational period  $T_i$  of the  $i^{\text{th}}$  segment represented by the abscissa of the obtained parabola's vertex, is determined from

$$T_i = -\frac{b}{2a} \quad (17)$$

$$T_i = -\frac{b}{2a} \quad (17)$$

The instantaneous rotational speed  $N_i$  is finally determined from the fine rotational period  $T_i$ :

$$N_i = \frac{60}{T_i} \quad (18)$$

#### *D. Measurement System*

Fig. 1 shows the fundamental principle of the imaging based rotational speed measurement system.

An image similarity evaluation algorithm, i.e. image correlation, is used to quantify the similarity

between the reference frame image and the subsequent images. The reference image is the average of the first 10 images acquired to ensure the reliability of the measurement. With a continuous comparison to the intensity distribution of the reference image, an image sequence is transformed to a time-domain signal indicating the similarity level of the sequential images. In Fig. 1,  $S(t)$  is the reconstructed time-domain signal indicating the similarity level between the reference image and the subsequent images. Under variable speed conditions, the rotating shaft exhibits dynamic behaviors and time variation characteristics, and thus the reconstructed signal indicating the similarity level  $S(t)$  is non-stationary. To address this problem, the signal  $S(t)$  is sliced to a successive of segments  $S_i(t)$  through a sliding short-time window function. Each segment of the similarity level signal does not fluctuate significantly during the time span of the short-time window and hence can be assumed as periodic. The periodicity of the segmented signal is in fact equal to the time of the shaft rotating for one complete revolution. The periodicity is obtained using periodicity determination methods, the CZT or PIAC, in this study.

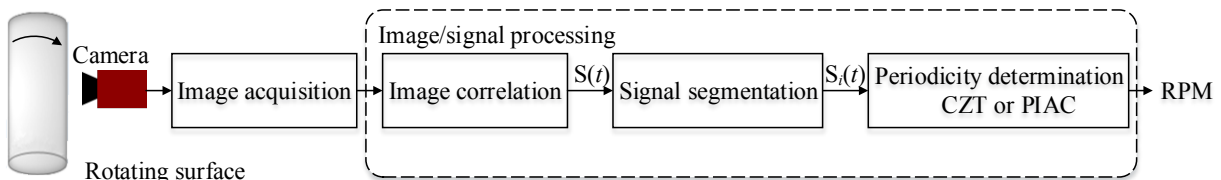


Fig. 1. Principle of the measurement system.

### III. EXPERIMENTAL RESULTS AND DISCUSSION

#### A. Experimental setup

Fig. 2 shows the experimental setup of the rotational speed measurement system. The steel rotating shaft with a diameter of 60 mm and an AC servo motor are connected together by a rigid coupling. The rotational speed is adjustable from 0 to 3000 RPM by manually regulating the input voltage

applied to the motor controller. The lens of the imaging sensor focuses on the side face of the shaft without any markers. The main specifications of the imaging sensor are summarized in Table I. The frame rate, image resolution and exposure time of the imaging sensor can be adjusted through a user interface. A strip-shaped LED light source is employed to control the illumination conditions. The shaft image data from the imaging sensor is fed into a laptop through a USB 3.0 cable. Fig. 3 illustrates typical images of the rotating shaft at the speed of 1000 RPM captured from the low-cost imaging device with a frame rate of 100 fps. It can be seen from Fig. 3 that the intensity distribution of the rotor image varies during rotational motion. With a continuous comparison to the intensity distribution of the reference image, the acquired image sequence is transformed into a time-domain signal indicating the similarity level of the sequential images. Fig. 4 presents the typical resulting similarity signal at a rotational speed of 1000 RPM. As expected, the signal is periodic due to the rotational motion of the rotor. In this study, the image/signal processing algorithms including image correlation, signal segmentation, periodicity determination and rotational speed calculation are realized on a laptop with Matlab (version R2017a). In this study a commercial laser tachometer (UNI-T, model UT372) with a maximum relative error of  $\pm 0.04\%$  with normalized standard deviation less than 0.04% was used to provide an independent reference to assess the measurement accuracy of the measured speed from the imaging system. To operate the laser tachometer, a reflective tape was fixed on the shaft. The acceptable measurement distance of the laser tachometer stated in the operation manual is 50-200 mm. In this setup the distance between the reflective tape surface and the inlet of the laser tachometer was 150 mm. In addition, a contact-type encoder (OMRON, model E6HZ-CWZ6C) with a resolution of 5000 pulses per revolution was fitted on the shaft to obtain additional independent reference data as a benchmark to evaluate the performance of the imaging system. In the experimental tests, the readings from the encoder and the laser

tachometer are all compared with the measured speed from the imaging system. In comparison to other speed estimation techniques in recently published literature, these two commercial tachometers can provide more accurate reference speeds to assess the performance of the proposed imaging system as they measure the speed directly rather than estimate the speed information from other types of signal, such as the motor current signal or vibration signal. In fact, the measurement accuracy of existing imaging approaches in recent literature is much lower than those of the rotary encoder and the laser tachometer, and thus they are not suitable to be chosen as reference instruments.

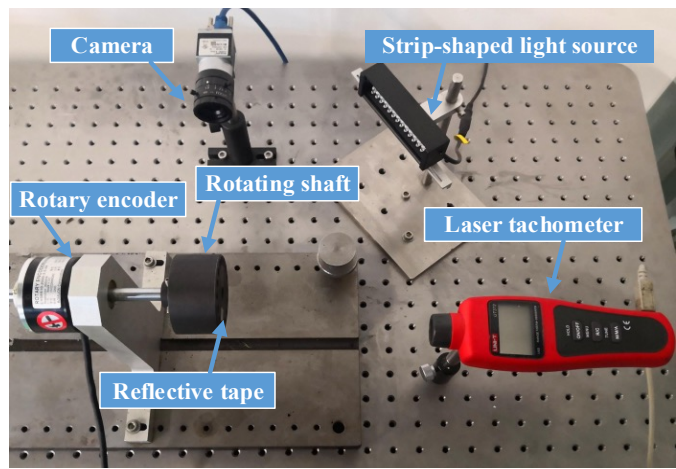


Fig. 2. Experimental setup of the rotational speed measurement system.

Table I. Main specifications of the imaging sensor

Mono/Colour	Maximum Frame rate (fps)	Maximum Image resolution	Minimum Exposure time ( $\mu$ s)	Interface
Mono	500	640 $\times$ 480	100	USB 3.0

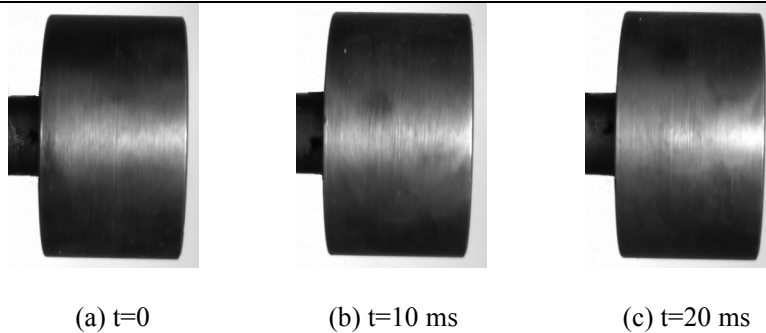


Fig. 3. Typical consecutive images of the rotating shaft at 1000 RPM.

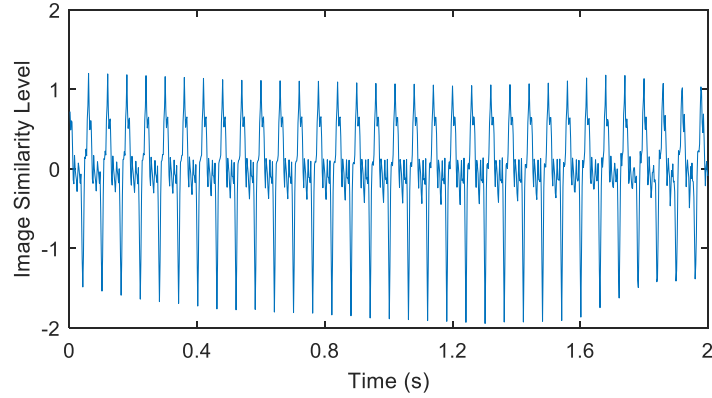


Fig. 4. Typical resulting signal of the image similarity level at 1000 RPM.

### *B. Performance analysis under constant speeds*

Before the performance assessment of the measurement system under dynamic operating conditions, a series of experimental tests was performed for constant rotational speeds under different experimental conditions in order to determine the optimal design parameters of the measurement system. For the low-cost imaging system, the periodicity determination algorithm, frame rate, image resolution, exposure time, illumination conditions, shooting angle are important parameters that may impact the measurement performance of the proposed system, and thus the effects of these factors are studied. The test conditions under which the measurement system was evaluated in this study are summarized in Table II. In this study the measurement accuracy is represented in terms of relative error between the measured speed and the reference speed. The repeatability of the system for a given condition is represented in terms of normalized standard deviation of the measured rotational speed. A total of 30 measurements under the same test condition were recorded for each repeatability test.

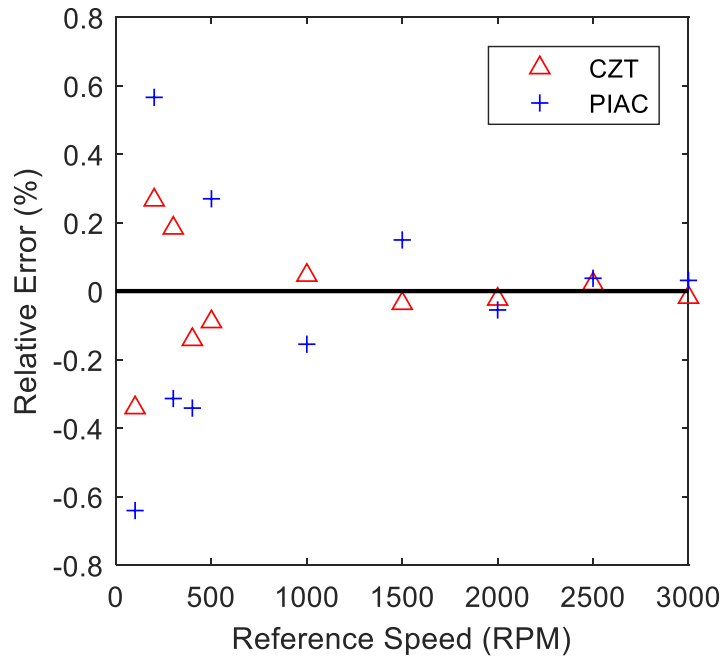
Table II. Test Programme

No	Signal processing algorithm	Frame rate (fps)	Image resolution (pixels)	Exposure time ( $\mu$ s)	Illumination (lux)	Angle ( $^{\circ}$ )	Speed (RPM)
I	CZT/PIAC	500	640×480	300	3000	0	100-3000
II	CZT	100/ 300/500	640×480	300	3000	0	
III	CZT	100	640×480, 320×240, 160×120, 80×60	300	3000	0	
IV	CZT	100	640×480	100/300/1000	3000	0	
V	CZT	100	640×480	300	1000/3000/ 5000	0	
VI	CZT	100	640×480	300	3000	0/10/20/30	

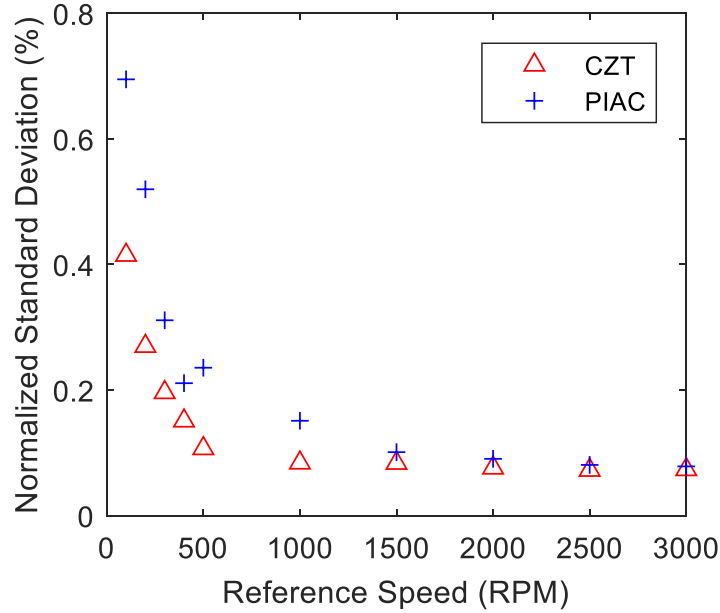
### 1) Comparison between the CZT and PIAC

In order to compare the performance of the periodicity determination algorithms, a series of experimental tests was carried out under the same conditions using the CZT and PIAC. Fig. 5 depicts a comparison between the measured speeds from the imaging system and the reference speeds from the laser tachometer over the range of 100-3000 RPM. It is evident that the measured speed is very close to the reference reading with a maximum error of  $\pm 0.65\%$  for either algorithm. As shown in Fig. 5, the two algorithms yield a similar trend. The relative error and normalized standard deviation decrease with the rotational speed. For instance, for the PIAC algorithm, the relative error is around 0.65% at the speed of 100 RPM with the normalized standard deviation of about 0.7%, while the error is significantly reduced to within  $\pm 0.1\%$  when the rotational speed increases. This result is also consistent with observations in other sets of experiments due to the fact that more rotating periods are available for signal processing at a higher speed during the same sampling time. It is also worth noting that the CZT performs better than the PIAC for the same speed in terms of accuracy and repeatability. At the speed of 100 RPM, the relative error of the CZT

is within  $\pm 0.4\%$  and the normalized standard deviation is around  $0.4\%$ , whereas the relative error is around  $0.65\%$  for the PIAC. The reason for this difference is that the low frame rate of the camera results in low resolution of the auto-correlation function and hence uncertainty in the sampling points for the parabolic interpolation of the peak in the auto-correlation function. Therefore, the CZT algorithm is employed for periodicity determination in the following study. In this study, a PC with Matlab software was used to implement image/signal processing instead of a dedicated device based on a microprocessor in order to focus our research effort on the fundamental principle and performance evaluation of the proposed methodology. It is expected that a highly integrated system capable of capturing image data and translating the data into desired measurements through embedded computing will be considered as the target device for instantaneous rotational speed measurement. For instance, a Raspberry Pi 4 Model B with a 1.5 GHz quad-core CPU and 4 GB memory is recommended for the practical implementation of the system for instantaneous rotational speed measurement.



(a) Relative error

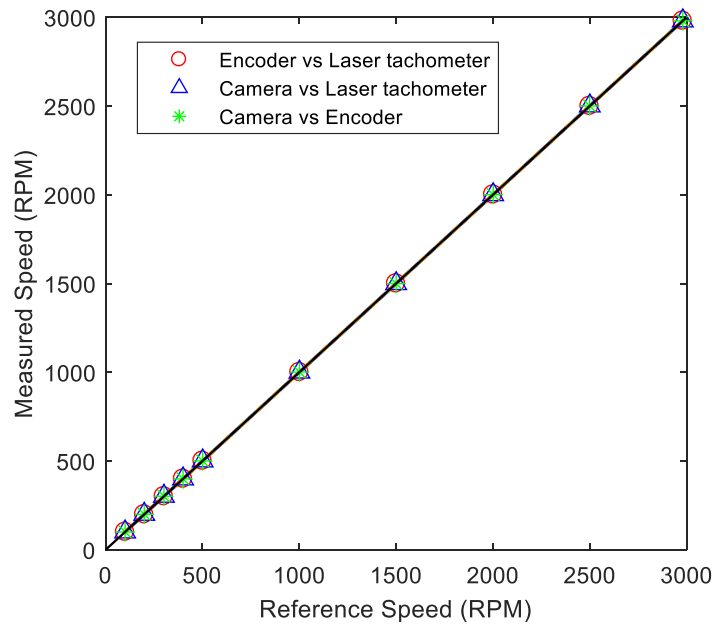


(b) Normalized standard deviation

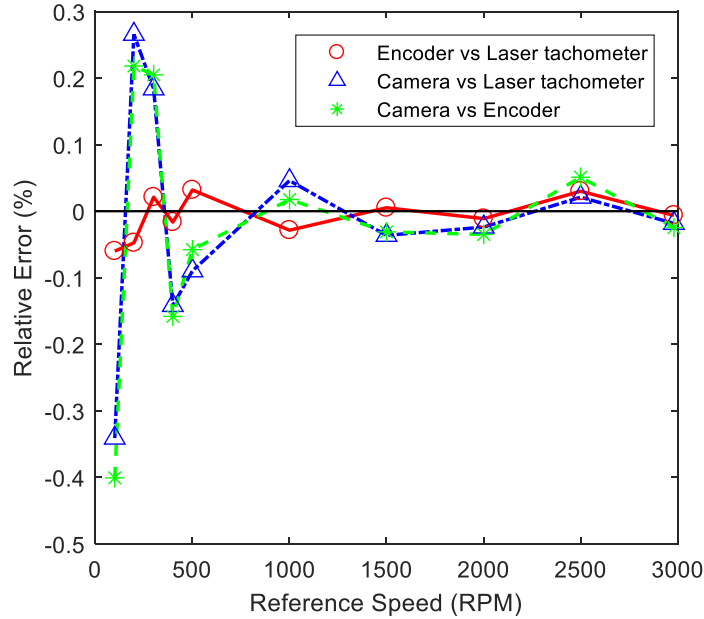
Fig. 5. Comparison of similarity signal processing algorithms.

In this paper, a series of experimental tests was conducted over the speed range from 100 to 3000 RPM using both the rotary encoder and the laser tachometer as reference instruments. The experimental results are shown in Fig. 6. It can be seen that the rotational speed from the laser tachometer is very close to that from the encoder with a maximum relative deviation of less than 0.06%, which is significantly lower than that of the imaging system. In other words, both the rotary encoder and the laser tachometer are capable of providing reliable reference speeds to assess the performance of the imaging system. However, the use of a rotary encoder is inconvenient due to hardware installation involved and the experimental environment. The encoder has to be coupled to the rotating shaft, which imposes restrictions on the maintenance and arrangement of the mechanical device. In some cases, rotational speed measurement using a rotary encoder may not be practical when the rotor is very large or inaccessible [5, 31]. In addition, the data acquisition system needs to be capable of acquiring and processing the encoder data stream and often requires dedicated measurement hardware [32]. For the imaging system, a free line of view (line of sight)

between the camera and the zone to be monitored is required. The installation of an encoder may lead to difficulties in the acquisition of rotor images. In comparison to the contact-type rotary encoder, the non-contact laser tachometer has a simpler structure and has little effect on the maintenance and layout of the experimental setup. Therefore, in subsequent experimental work the laser tachometer is selected as the reference device. In our previous work as outlined in the introduction section, a marker based imaging system has been proposed for rotational speed measurement through image similarity evaluation and spectral analysis [19, 20]. The system is capable of providing rotational speed measurement with a relative error of  $\pm 0.6\%$  over a speed range from 100 to 900 RPM. As shown in Fig. 6, the relative error of the proposed system is within  $\pm 0.3\%$  over a speed range of 100-3000 RPM. In other words, the proposed imaging system is capable of measuring rotational speed more accurately over a wider speed range than the marker based system. In addition, this measurement technique has potentially a wider applicability as no marker is required on the target object.



(a) Measured speed vs reference speed



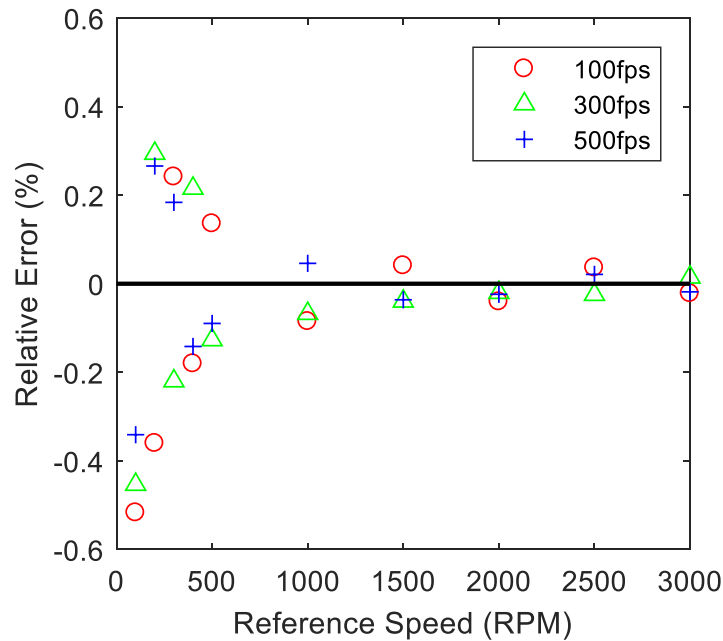
(b) Relative error of the measured rotational speed

Fig. 6. Comparison between the measured speed through digital imaging and the reference speed.

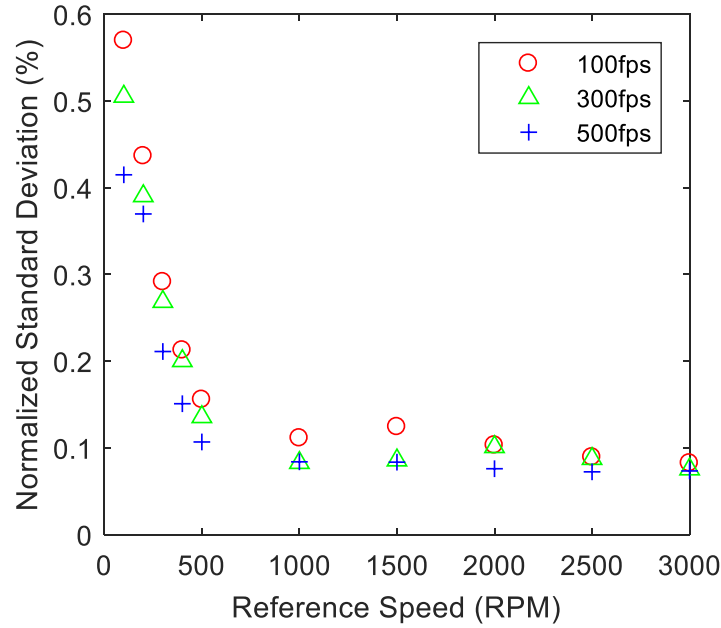
## 2) Effect of Frame Rate

A series of experimental tests was conducted with three different frame rates, 100 fps, 300 fps and 500 fps, respectively, to quantify the effect of the frame rate on the measurement system performance. As shown in Fig. 7, the comparison between the measured and reference speeds demonstrates that the proposed system, even with the frame rate of 100 fps, is capable of providing accurate and reliable measurement over the whole speed range. The relative error is within  $\pm 0.6\%$  whilst the normalized standard deviation is no greater than 0.6% under all test conditions. This result verifies the feasibility and potential of a low-cost camera with a low frame rate for rotational speed measurement. In addition, the accuracy and repeatability are both improved as the rotational speed increases. It is important to note that the frame rate limits the measurement range of the rotational speed. In order to avoid temporal aliasing, the frame rate of the camera should be at least twice the rotational frequency according to the Nyquist sampling criterion. In other words, the

maximum measurable rotational frequency for a given frame rate ( $f_s$ ) is  $f_s/2$ . According to equation (3), the rotational speed is 60 times the rotational frequency. Therefore, the maximum measurable speed for the frame rate ( $f_s$ ) is  $60 \times f_s/2 = 30 \times f_s$  RPM. In the experimental tests, the maximum speed available on the test rig is 3000 RPM. The available frame rate should be no lower than 100 fps ( $3000/60 \times 2$ ). In addition, the maximum frame rate of the imaging sensor is 500 fps. Therefore, the acceptable range of the frame rate is [100 fps, 500 fps]. In this case, the measured rotational speeds with a relative error less than  $\pm 5\%$  are deemed as reliable measurements. If the frame rate is lower than 100 fps, the relative error will be significantly larger than  $\pm 5\%$  due to temporal aliasing. As expected, a higher sampling frequency generates more accurate and repeatable results due to the smoother signal with the increasing sampling points. Consequently, a higher frame rate is essential for higher measurement accuracy and better repeatability as well as extending the measurable speed range.



(a)Relative error

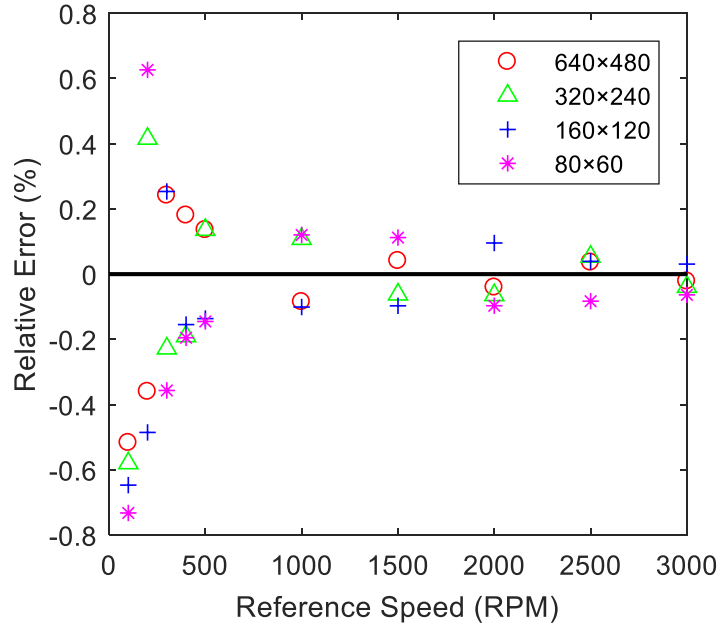


(b) Normalized standard deviation

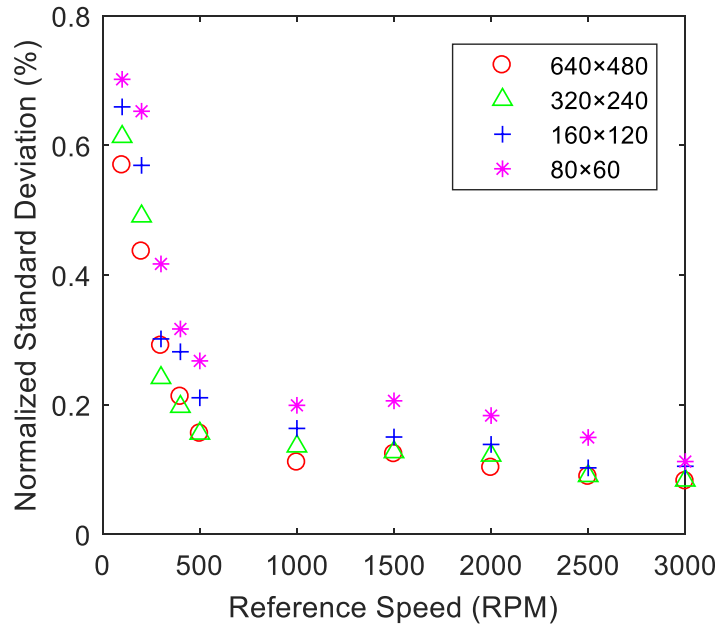
Fig. 7. Results for different frame rates.

### 3) Effect of image resolution

In order to study the effect of image resolution, different resolutions, including  $640 \times 480$ ,  $320 \times 240$ ,  $160 \times 120$  and  $80 \times 60$ , were tested. Fig. 8 indicates that the rotational speed can be measured accurately and reliably even when the image resolution is as low as  $80 \times 60$  pixels. Under this circumstance the measurement system has a shorter computational time and hence fast system response. However, when the image resolution is lower than  $80 \times 60$  pixels, the relative error of the measured rotational speed is larger than  $\pm 5\%$  due to fewer pixel data and insufficient information extracted from the acquired images. Therefore, the image resolution should be no lower than  $80 \times 60$  pixels in order to maintain reasonable accuracy in rotational speed measurement. As expected, the captured images with the highest resolution has the best performance. This outcome is attributed to the fact that an increasing volume of pixel data is used to sense the changes in the intensity distribution due to the rotational motion of the shaft, improving the determination accuracy of the correlation coefficient.



(a) Relative error



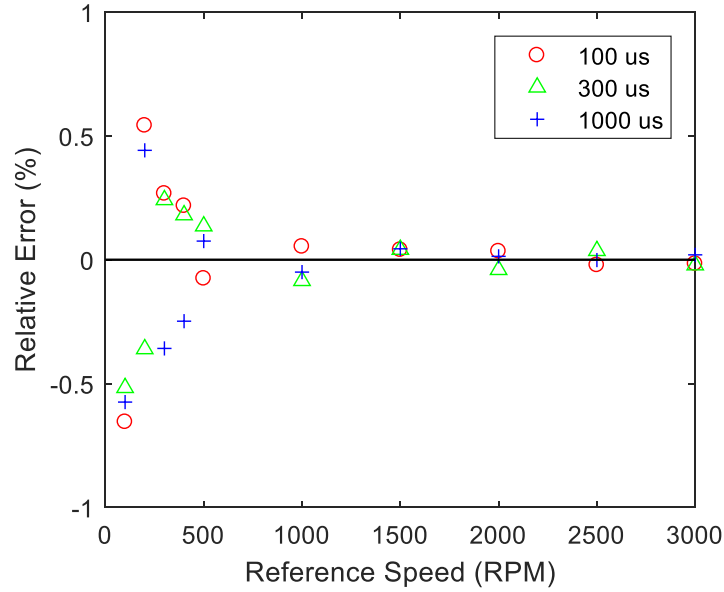
(b) Normalized standard deviation

Fig. 8. Results for different image resolutions.

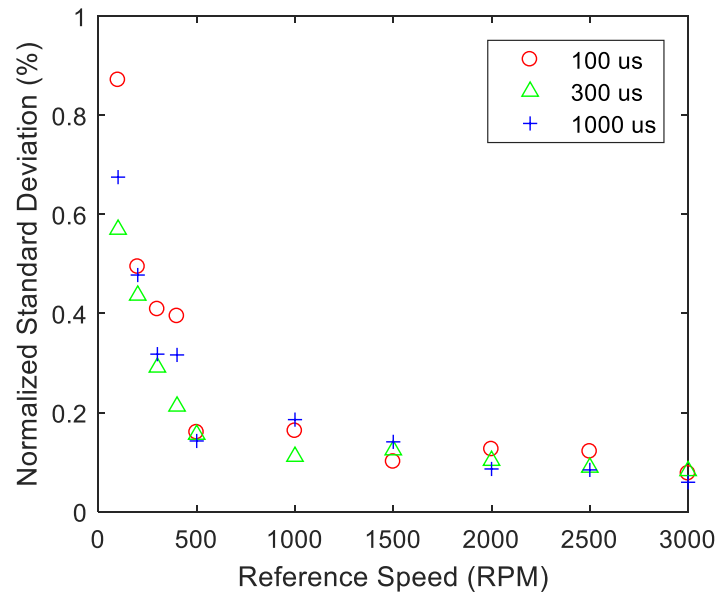
#### 4) Effect of exposure time

In order to explore the effect of exposure time on the measurement performance, experimental tests were conducted with different exposure times, namely short exposure (100  $\mu$ s), normal exposure (300  $\mu$ s) and long exposure (1000  $\mu$ s). As depicted in Fig. 9, the relative error and

normalized standard deviation with short and long exposure times are larger than that with normal exposure time. This is because a short exposure time will result in under-exposure and poor image contrast, generating the loss of motion information and hence low measurement performance. On the other hand, the acquired images with a long exposure time exhibits distinct motion blurring due to the superposition of the image intensities, which causes an increasing error in the determination of the similarity level of consecutive images. It is worth noting that although motion blur reduces the performance of the measurement system, this performance degradation introduced by over-exposure is acceptable. The images with the exposure time of 1000  $\mu\text{s}$  exhibits motion blur, especially at a higher rotational speed. However, the standard deviation, shown in Fig. 9, is still lower than 0.7% over the whole speed range, which demonstrates that the measurement system is robust enough for motion blur. To ensure the best measurement performance of the proposed system, the exposure time of the imaging sensor should be properly set according to the maximum rotational speed of the shaft and illumination conditions in real applications. In this experiment, the illumination intensity is kept at 3000 lux. The exposure time of 300  $\mu\text{s}$  is sufficient for capturing clear images of the shaft surface with good contrast for the maximum rotational speed of 3000 RPM.



(a) Relative error



(b) Normalized standard deviation

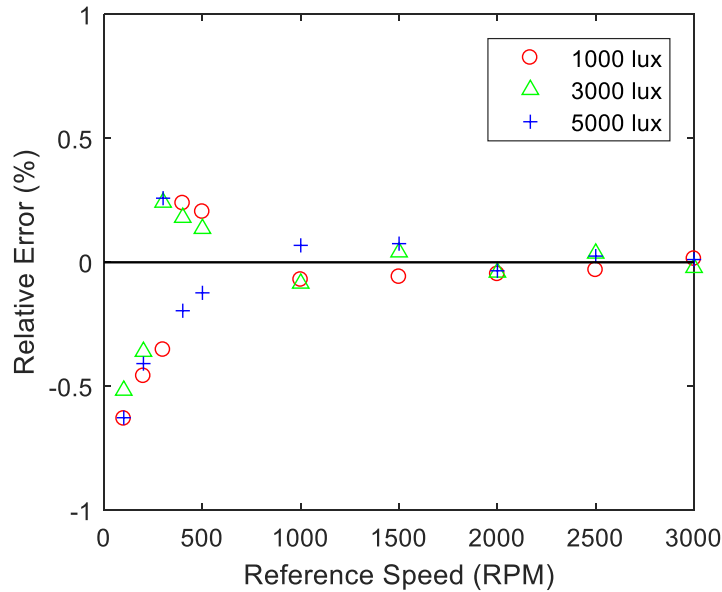
Fig. 9. Results for different exposure times.

### 5) Effect of illumination conditions

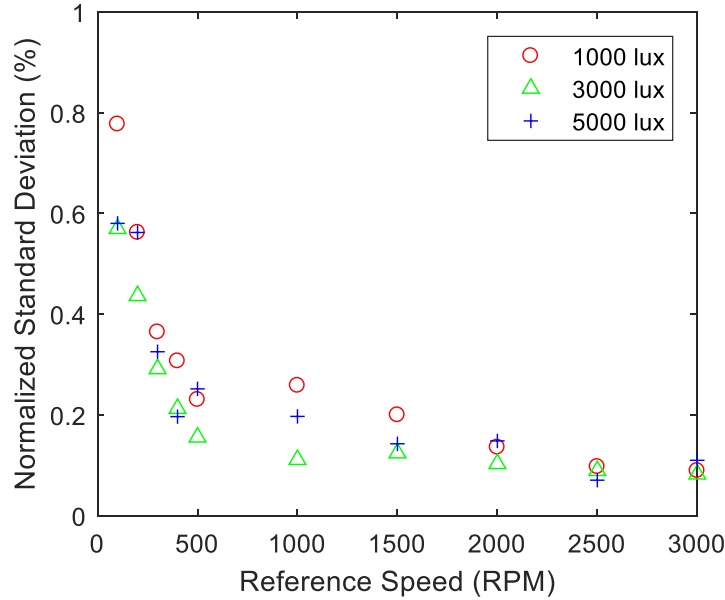
Experimental tests were carried out to reveal the effect of lighting conditions. With the help of a strip-shaped LED light source, the illumination conditions were adjusted to weak (1000 lux), normal (3000 lux) and strong (5000 lux) light, respectively. The results shown in Fig. 10 indicate the measurement system has a better performance under normal illumination conditions. The

normalized standard deviation with weak or strong illumination conditions is slightly larger than that with normal light. Illumination conditions are closely related to the image quality, which affect grayscale distribution characteristics of recorded images. Poor image contrast under the weak and strong light conditions results in information loss of shaft surface texture and hence uncertainty in the determination of image similarity level. It also can be seen that the measurement accuracy and reliability are still satisfactory under different illumination intensities. This means that the measurement system is robust enough under weak and strong illumination conditions.

Due to the limitations of the experimental setup, the adjustable ranges of exposure time and illumination conditions are [100  $\mu$ s, 1000  $\mu$ s] and [1000 lux, 5000 lux], respectively. Experimental results shown in Fig. 9 and Fig. 10 illustrate that the proposed imaging system can measure the rotational speed accurately and reliably over the exposure time range of 100-1000  $\mu$ s and over the illumination range of 1000-5000 lux. The measurement system is robust enough for a range of exposure time and illumination intensity except under extreme conditions.



(a) Relative error



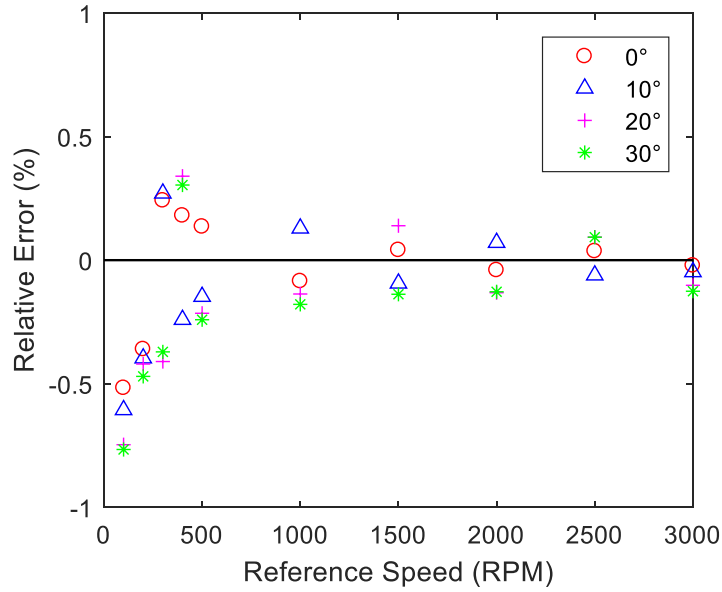
(b) Normalized standard deviation

Fig. 10. Results under different illumination conditions.

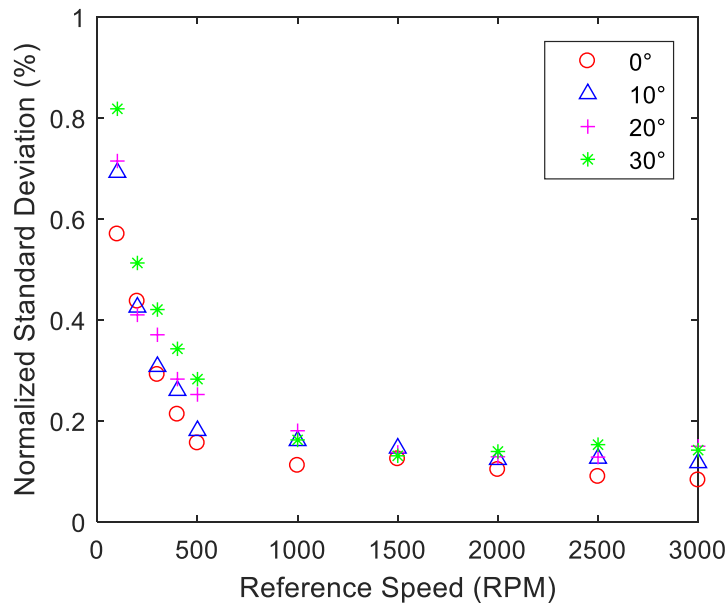
#### 6) Effect of photographic angle

In practical applications, the optical axis of the imaging sensor may not be perpendicular to the axis of the shaft. For this reason it is necessary to evaluate the effect of the camera angle on the measurement performance. Experimental tests were conducted under four different shooting angles: 0°, 10°, 20° and 30°. The shooting angle between the optical axis of the imaging device and the moving surface of the shaft is adjustable with the aid of a supporting frame. It is worth noting that, when the viewing angle is larger than 30°, the rotor is no longer in the field of view of the imaging sensor, and thus the rotational speed measurement is no longer possible. Therefore, the acceptable range of photographic angle is [0°, 30°]. The results shown in Fig. 11 suggest that the measurement system performs the best when the optical axis of the imaging device is perpendicular to the shaft surface due to the smallest distortion of the imaging device. Both the relative error and normalized standard deviation increase with the shooting angle, which is attributed to greater image distortion and the change in the field of view of the imaging device. When the imaging sensor plane is not

parallel with the shaft surface, the ideal linear correspondence between the physical point and imaged point may be distorted, resulting in additional measurement errors. It should be noted that the relative error and standard deviation are consistently less than 1% even when the shooting angle is  $30^\circ$ , which demonstrates that the measurement system is robust enough for a range of shooting angles.



(a) Relative error



(b) Normalized standard deviation

Fig. 11. Results for different shooting angles.

### C. Dynamic measurement of instantaneous angular speed

The effectiveness of the proposed system for dynamic measurement of instantaneous rotational speed was verified in comparison to the reference speeds from the laser tachometer. Experimental tests were carried out by gradually increasing the rotational speed and introducing step changes in the rotational speed from 1000 RPM to 2000 RPM. As per the experimental results in Section III. B, the optimal parameters of the imaging system are set to obtain the best measurement performance and are summarized in Table III. In terms of dynamic rotational speed measurement, the acceptable ranges of influence factors are the same as those under steady conditions. When these parameters are out of the acceptable ranges, the imaging system is incapable of providing acceptable measurement of instantaneous speed with a relative error within  $\pm 5\%$  due to insufficient information in the acquired images. In these experimental tests, CZT is selected to determine the periodicity of the segmented signal indicating the similarity level.

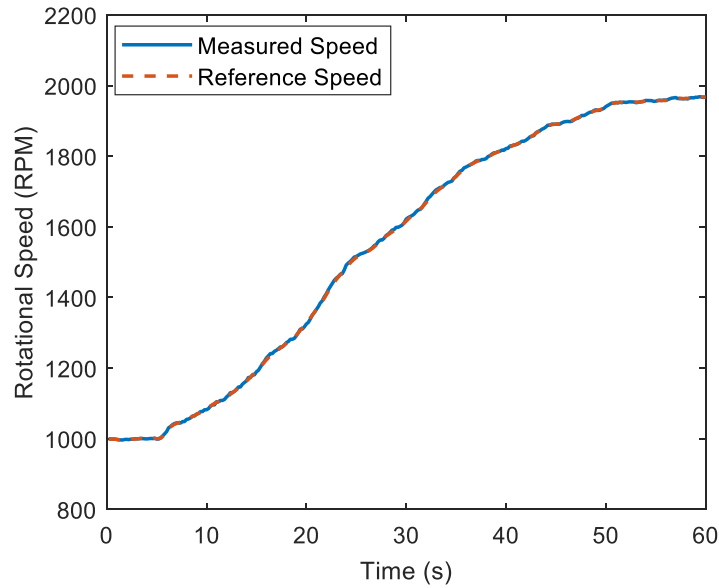
Table III. Optimal parameters of the imaging system

<b>Frame rate (fps)</b>	<b>Image resolution (pixels)</b>	<b>Exposure time (<math>\mu</math>s)</b>	<b>Illumination (lux)</b>	<b>Angle (<math>^{\circ}</math>)</b>
500	640 $\times$ 480	300	3000	0

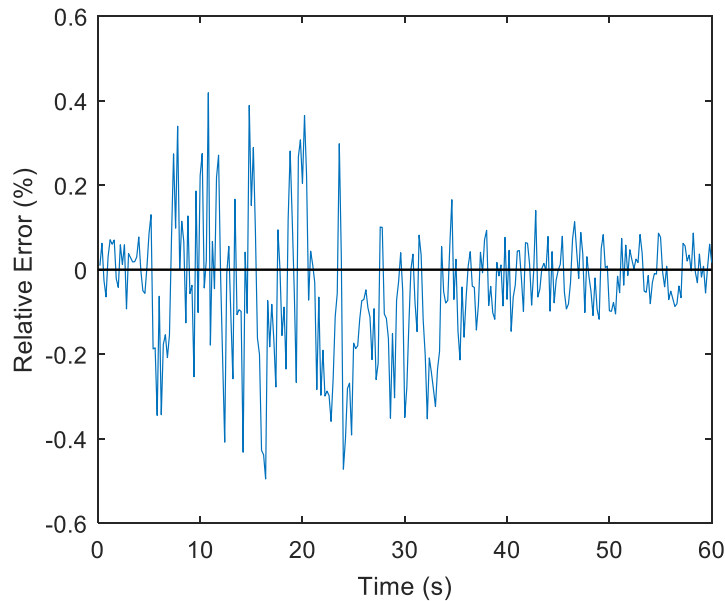
#### 1) Gradual increase in speed

The speed increases gradually from 1000 RPM to 2000 RPM over a period of 60 s. As shown in Fig. 12, the reference speed from the laser tachometer coincides well with the measured instantaneous rotational speed from the imaging system. As can be seen, there is an acceleration process from the 6<sup>th</sup> second to the 50<sup>th</sup> second. The maximum relative error is less than  $\pm 0.1\%$  before the 7<sup>th</sup> second, then increases to a higher level ( $\pm 0.5\%$ ) due to the rising speed. When the shaft reaches the steady-state operating condition at the speed of 2000 RPM, the error decreases to  $\pm 0.1\%$ . The results demonstrate that the imaging system is capable of providing the measurement of

instantaneous rotational speed with high accuracy under non-stationary operating conditions. As expected, the accuracy under dynamic conditions is lower than that under steady speed conditions due to the non-stationary nature of the signal indicating the similarity level. Moreover, the measurement error becomes larger when the speed varies more rapidly due to the fact that the segmented signal of similarity level is less periodic under such conditions.



(a) Measured speed versus the reference speed

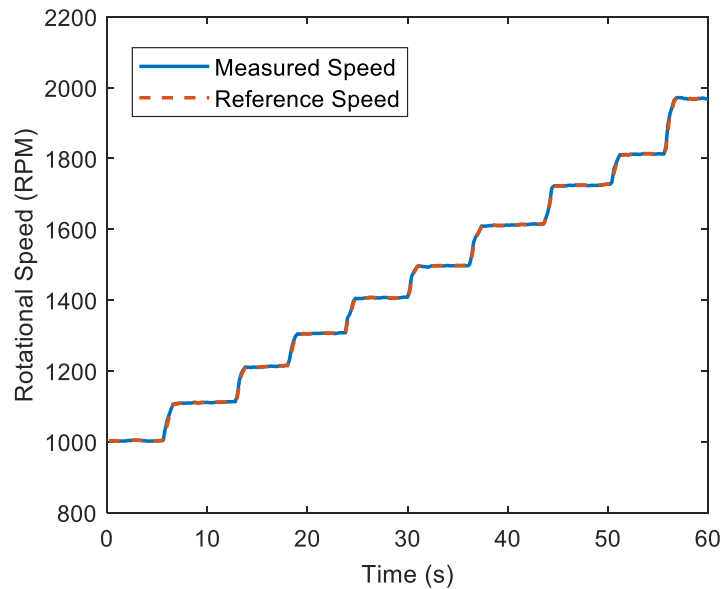


(b) Relative error of the measured instantaneous speed

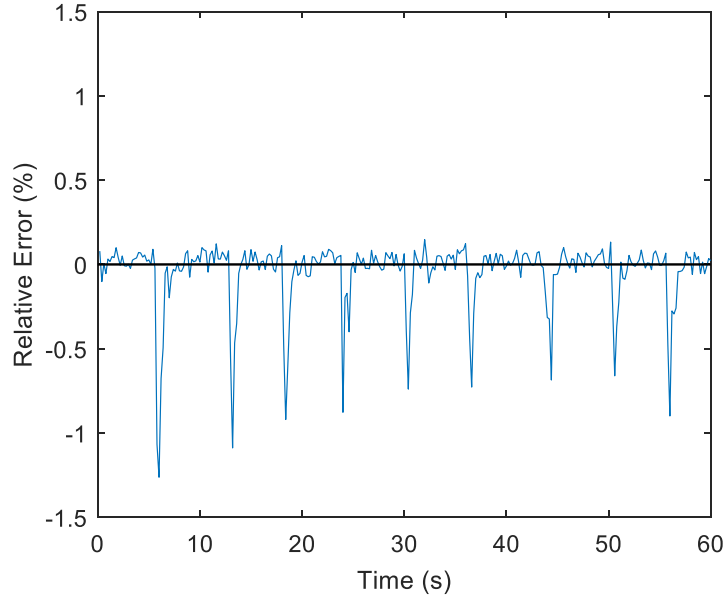
Fig. 12. Results for generally increasing rotational speed.

## 2) Step-changes in speed

The rotational speed is controlled to present step changes over the range from 1000 to 2000 RPM. As shown in Fig. 13, the reference and measured speed curves are consistent with each other, although the measurement errors at the step increase points are slightly larger. It is clear that the reference speeds from the reference metering device around step increase points are consistently larger than the measured rotational speeds from the imaging system due to different measuring principles. This is expected as the imaging system needs to record multiple images of shaft side surface and converts them into a time domain signal for determining the rotational speed and thus requires a short time interval to correctly track sudden changes in rotational speed. The experimental results also suggest that the low-cost imaging system correctly identifies the dynamic characteristics of the instantaneous rotational speed under non-stationary conditions.



(a) Measured speed versus the reference speed



(b) Relative error of the measured instantaneous speed.

Fig. 13. Results for step changes in rotational speed.

#### *D. Elapsed time comparison of the imaging system and the laser tachometer*

Table IV outlines the elapsed time of each measurement cycle using the proposed experimental imaging system with reference to the laser tachometer. The commercial laser tachometer can provide 5 rotational speed values per second. For the imaging system, the response time depends on the frame rate and image resolution for a given computer system. The lower frame rate and reduced image resolution entail lower computational complexity and hence faster system response, but at the expenses of lower measurement accuracy due to the decreasing volume of data to process. When the frame rate and image resolution are 500 fps and  $640 \times 480$  pixels, respectively, the total processing time of each measurement cycle is found to be 0.64 s for the computer system used (Intel(R) Core(TM) i5-8250U 1.60 GHz CPU, 4 GB RAM, MS Windows 8). By contrast, when the frame rate and image resolution are 100 fps and  $80 \times 60$  pixels, respectively, the elapsed time of each measurement cycle is 0.029 s. The measured rotational speed with respect to such short processing times can be considered as “instantaneous”. The processing time is expected

comparable or less than these values if an appropriate microprocessor such as Raspberry Pi 4 with suitable software is used. This scale of response time can meet the requirements of condition monitoring and real-time control of mechanical systems. It is clear that the exposure time, illumination conditions and viewing angle have little effect on the response time as they do not influence the computational complexity of the imaging method.

Table IV. Elapsed time comparison of the imaging system and the laser tachometer

Rotational speed measurement system	Imaging system (500 fps, 640×480)	Imaging system (100 fps, 80×60)	Laser tachometer
Elapsed time of each measurement cycle (s)	0.64	0.029	0.2

#### IV. CONCLUSIONS

The measurement of instantaneous rotational speed has been implemented using a low-cost imaging device and image processing techniques in this research study. Experimental results under a range of controlled test conditions have suggested that the rotational speed measurement system without the use of any markers on the object in motion performs well under steady and dynamic operating conditions. For constant speed measurement, the low-cost imaging device yields a relative error of no greater than  $\pm 0.6\%$  over the speed range of 100-3000 RPM. For rotational speed 1000 RPM and given a sufficient frame rate and image resolution, both the measurement error and the normalized standard deviation are consistently within  $\pm 0.1\%$ . The relative error in the case of gradual increase in rotational speed is less than  $\pm 0.5\%$  whilst a maximum error of -1.4% is obtained in case of step-changes in speed over the speed range from 1000 RPM to 3000 RPM. It has been found that the CZT is a more suitable algorithm for periodicity determination than the PIAC under a low frame rate. The results presented have indicated that the system performance is still satisfactory even if the image resolution is as low as 80×60 pixels. It is also worth noting that illumination conditions and exposure time have little impact on the measurement

results and the measurement system is robust even though the optical axis of the imaging device is not perpendicular to the shaft side surface. Further work will focus on the performance assessment of the measurement system on industrial trials. In addition, smart condition monitoring and fault diagnosis of rotational machines by analyzing the variations in the instantaneous rotational speed using the imaging system will be conducted in the near future.

### **ACKNOWLEDGMENT**

The authors wish to acknowledge the National Natural Science Foundation of China (No. 51375163), State Key Laboratory of Alternate Electrical Power Systems with Renewable Energy Sources, North China Electric Power University (LAPS2019-18), the Fundamental Research Funds for the Central Universities (No. 2017XS157), and the North China Electric Power University Joint Graduate Program for providing financial support for this research. Shuai Zhang would like to thank the IEEE Instrumentation and Measurement Society for 2016 Graduate Fellowship Award.

### **References**

- [1] A. K. Jardine, D. Lin and D. Banjevic, “A review on machinery diagnostics and prognostics implementing condition-based maintenance,” *Mech. Syst. Signal Pr.*, vol. 20, no. 7, pp. 1481–1510, 2006.
- [2] J. Yang, L. Pu, Z. Wang, Y. Zhou and X. Yan, “Fault detection in a diesel engine by analysing the instantaneous angular speed,” *Mech. Syst. Signal Pr.*, vol. 15, no. 3, pp. 549–564, 2001.
- [3] S. Nandi, H. A. Toliyat and X. Li, “Condition monitoring and fault diagnosis of electrical motors—a review,” *IEEE Trans. Energy Convers.*, vol. 20, no. 4, pp. 719–729, 2005.

- [4] S. Lu, Q. He and F. Kong, “Stochastic resonance with Woods-Saxon potential for rolling element bearing fault diagnosis,” *Mech. Syst. Signal Pr.*, vol. 45, no. 2, pp. 488–503, 2014.
- [5] J. Urbanek, T. Barszcz and J. Antoni, “A two-step procedure for estimation of instantaneous rotational speed with large fluctuations,” *Mech. Syst. Signal Pr.*, vol. 38, no. 1, pp. 96–102, 2013.
- [6] Y. Li, F. Gu, G. Harris and A. Ball, “The measurement of instantaneous angular speed,” *Mech. Syst. Signal. Pr.*, vol. 19, pp. 786–805, 2005.
- [7] Y. S. Didosyan, H. Hauser, H. Wolfmayr, J. Nicolics and P. Fulmek, “Magneto-optical rotational speed sensor,” *Sens. Actuators A, Phys.*, vol. 106, nos. 1–3, pp. 168–171, 2003.
- [8] L. Wang, Y. Yan, Y. Hu and X. Qian, “Rotational speed measurement through electrostatic sensing and correlation signal processing,” *IEEE Trans. Instrum. Meas.*, vol. 63, no. 5, pp. 1190–1199, 2014.
- [9] S. Yu and X. Zhang, “A data processing method for determining instantaneous angular speed and acceleration of crankshaft in an aircraft engine-propeller system using a magnetic encoder,” *Mech. Syst. Signal Pr.*, vol. 24, no. 4, pp. 1032–1048, 2010.
- [10] D. Shi, P. J. Unsworth and R. X. Gao, “Sensorless speed measurement of induction motor using Hilbert transform and interpolated fast Fourier transform,” *IEEE Trans. Instrum. Meas.*, vol. 55, no. 1, pp. 290–299, 2006.
- [11] M. Aiello, A. Cataliotti and S. Nuccio, “An induction motor speed measurement method based on current harmonic analysis with the chirp-Z transform,” *IEEE Trans. Instrum. Meas.*, vol. 54, no. 5, pp. 1811–1819, 2005.

- [12] H. Lin and K. Ding, "A new method for measuring engine rotational speed based on the vibration and discrete spectrum correction technique," *Measurement* vol. 46, no. 7, pp. 2056–2064, 2013.
- [13] J. Zhong, S. Zhong, Q. Zhang, Z. Peng, S. Liu and Y. Yu, "Vision-based measurement System for instantaneous rotational speed monitoring using linearly varying-density fringe pattern," *IEEE Trans. Instrum. Meas.*, vol. 67, no. 6, pp. 1434–1445, 2018.
- [14] J. Zhong, S. Zhong, Q. Zhang and Z. Peng, "Measurement of instantaneous rotational speed using double sine-varying-density fringe pattern," *Mech. Syst. Signal Pr.*, vol. 103, no. 3, pp. 117–130, 2018.
- [15] H. Kim, Y. Yamakawa, T. Senoo and M. Ishikawa, "Visual encoder: robust and precise measurement method of rotation angle via high-speed RGB vision," *Opt. Express.*, vol. 24, no. 12, pp. 13375–13386, 2016.
- [16] X. Zhang, J. Chen, Z. Wang, N. Zhan and R. Wang, "Digital image correlation using ring template and quadrilateral element for large rotation measurement," *Opt. Lasers Eng.*, vol. 50, no. 7, pp. 922–928, 2012.
- [17] W. Li, J. Jin, X. Li, and B. Li, "Method of rotation angle measurement in machine vision based on calibration pattern with spot array," *Appl. Opt.*, vol. 49, no. 6, pp. 1001–1006, 2010.
- [18] J. Guo, C. Zhu, S. Lu, D. Zhang and C. Zhang, "Vision-based measurement for rotational speed by improving Lucas-Kanade template tracking algorithm," *Appl. Optics.*, vol. 55, no. 25, pp. 7186–7194, 2016.
- [19] Y. Wang, L. Wang and Y. Yan, "Rotational speed measurement through digital imaging and image processing," in *Proc. IEEE Int. Instrum. Meas. Technol. Conf.*, Torino, Italy, May 2017, pp. 260–265.

- [20] T. Wang, Y. Yan, L. Wang and Y. Hu, "Rotational speed measurement through image similarity evaluation and spectral Analysis," *IEEE Access*, vol. 6, pp. 46718-46730, 2018.
- [21] T. Wang, L. Wang, Y. Yan, and S. Zhang, "Rotational speed measurement using a low-cost imaging device and image processing algorithms," in *Proc. IEEE Int. Instrum. Meas. Technol. Conf.*, Houston, USA, May 2018, pp. 1900–1905.
- [22] Y. Wang, Y. Yan and L. Wang, "Vibration measurement using a low-cost imaging sensor and image processing techniques," in *J. Phys., Conf. Ser.*, Belfast, UK, 3-6 Sept. 2018, pp. 222012.
- [23] R. Szeliski, "Computer Vision: Algorithms and Applications," Springer, New York, 2010.
- [24] A. Kaur, L. Kaur and S. Gupta, "Image recognition using coefficient of correlation and structural similarity index in uncontrolled environment," *Intel. J. Comput. Appl.*, vol. 59, no. 5, pp. 32–39, 2012.
- [25] B. Pan, K. Qian, H. Xie, and A. Asundi, "Two-dimensional digital image correlation for in-plane displacement and strain measurement: a review," *Meas. Sci. Technol.*, vol. 20, pp. 062001, 2009.
- [26] W. Zhang, C. Wang and Y. Wang, "Parameter selection in cross-correlation-based velocimetry using circular electrostatic sensors," *IEEE Trans. Instrum. Meas.*, vol. 59, no. 5, pp. 1268–1275, 2010.
- [27] D. Granados-Lieberman, R. J. Romero-Troncoso, E. Cabal-Yepez, R. A. Osornio-Rios and L. A. Franco-Gasca, "A real-time smart sensor for high-resolution frequency estimation in power systems," *Sensors*, vol. 9, no. 9, pp. 7412–7429, 2009.

- [28] M. Aiello, A. Cataliotti, and S. Nuccio, "A comparison of spectrum estimation techniques for nonstationary signals in induction motor drive measurements," *IEEE Trans. Instrum. Meas.*, vol. 54, no. 6, pp. 2264–2271, 2005.
- [29] R. Moddemeijer, "On the determination of the Position of Extrema of Sampled Correlators," *IEEE Signal Process. Mag.*, vol. 39, no. 1, pp. 216–219, 1991.
- [30] S. Lu, G. Qian, Q. He, F. Liu, Y. Liu and Q. Wang, "Insitu motor fault diagnosis using enhanced convolutional neural network in an embedded system," *IEEE Sensors Journal*, DOI: 10.1109/JSEN.2019.2911299, 2019.
- [31] F. Combet and R. Zimroz, "A new method for the estimation of the instantaneous speed relative fluctuation in a vibration signal based on the short timescale transform," *Mech. Syst. Signal Pr.*, vol. 23, no. 4, pp. 1382–1397, 2009.
- [32] C. Peeters, Q. Leclère, J Antoni, P. Lindahl, J Donald, S. Leeb, J Helsen, "Review and comparison of tachless instantaneous speed estimation methods on experimental vibration data," *Mech. Syst. Signal Pr.*, vol. 129, pp. 407–436, 2019.